Environmental Science and Pollution Research (2023) 30:50520–50536
https://doi.org/10.1007/s11356-023-25846-4

RESEARCH ARTICLE

Metal organic framework–derived recyclable magnetic coral Co@Co_3O_4/C for adsorptive removal of antibiotics from wastewater

Puja Bhattacharyya[1] · Prathu Raja Parmar[2] · Sanchari Basak[1] · Kashyap Kumar Dubey[3] · Soumyaditya Sutradhar[4] · Dipankar Bandyopadhyay[2,5,6] · Sandip Chakrabarti[1]

Received: 9 October 2022 / Accepted: 6 February 2023 / Published online: 16 February 2023

Abstract

The menace posed by antibiotic contamination to humanity has increased due to the absence of efficient antibiotic removal processes in the conventional waste water treatment methods from the hospitals, households, animal husbandry, and pharma industry. Importantly, only a few commercially available adsorbents are magnetic, porous, and have the ability to selectively bind and separate various classes of antibiotics from the slurries. Herein, we report the synthesis of a coral-like Co@Co_3O_4/C nanohybrid for the remediation of three different classes of antibiotics — quinolone, tetracycline, and sulphonamide. The coral like Co@Co_3O_4/C materials are synthesized via a facile room temperature wet chemical method followed by annealing in a controlled atmosphere. The materials demonstrate an attractive porous structure with an excellent surface-to-mass ratio of 554.8 $m^2\ g^{-1}$ alongside superior magnetic responses. A time-varying adsorption study of aqueous nalidixic acid solution on Co@Co_3O_4/C nanohybrids indicates that these coral-like Co@Co_3O_4/C nanohybrids could achieve a high removal efficiency of 99.98% at pH 6 in 120 min. The adsorption kinetics data of Co@Co_3O_4/C nanohybrids follow a pseudo-second-order reaction kinetics suggesting a chemisorption effect. The adsorbent has also shown its merit in reusability for four adsorption-desorption cycles without showing significant change in the removal efficiency. More in-depth studies validate that the excellent adsorption capability of Co@Co_3O_4/C adsorbent attributing to the electrostatic and π–π interaction between adsorbent and various antibiotics. Concisely, the adsorbent manifests the potential for the removal of a wide range of antibiotics from the water alongside showing their utility in the hassle-free magnetic separation.

Keywords MOF · Coral nanostructures · Magnetic · Antibiotics · Adsorption

Dipankar Bandyopadhyay and Sandip Chakrabarti contributed equally to the manuscript.

Responsible Editor: Angeles Blanco

✉ Sandip Chakrabarti
schakrabarti@amity.edu

[1] Amity Institute of Nanotechnology, Amity University Uttar Pradesh, Noida 201303, India

[2] Department of Chemical Engineering, Indian Institute of Technology Guwahati, Guwahati, Assam 781039, India

[3] School of Biotechnology, Jawaharlal Nehru University, New Delhi 110067, India

[4] Department of Physics, Jadavpur University, Kolkata, West Bengal 700032, India

[5] Centre for Nanotechnology, Indian Institute of Technology Guwahati, Guwahati, Assam 781039, India

[6] School of Health Sciences and Technology, Indian Institute of Technology Guwahati, Guwahati, Assam 781039, India

Abbreviations

NAL	Nalidixic acid
TC	Tetracycline
CIP	Ciprofloxacin
SMX	Sulfamethoxazole

Introduction

Antibiotic contamination in aquatic life has emerged as one of the most pressing worldwide issues in recent years, posing a grave threat to the survival of the human species by enabling microbes to develop antibiotic resistance (Ahmed and Hameed 2018). Several lifesaving antibiotics are becoming ineffective during the need of the hour pursuing limitations associated with the management of wastewater from the pharma industry (Wang et al. 2020b). This is even more alarming from the stance of the recent COVID-19 pandemic, which has exposed the world population to ubiquitous and

routine usage of antibiotics (Zhou et al. 2020). Importantly, pharmaceutical wastewater also contain other hazardous chemicals, which degrade slowly and accumulate rapidly in the human body (Ahmed and Hameed 2018). The other sources of antibiotic pollution are hospitals, households, and animal husbandry (Cao et al. 2017). It is now well known that synthetic pharmaceutical compounds (SPC) have severe phyto-toxicological and genotoxicity, endocrine disruption, and aquatic toxicity in the environment (Zhao et al. 2019). Nalidixic acid (NAL) is a well-known SPC. This derivative of orally administered non-fluorinated quinolone is used to cure infections of the urinary tract caused by sensitive gram-negative bacteria, such as *Escherichia coli*, *Enterobacter species*, *Klebsiella species*, and *Proteus species* (Meras et al. 2000).

Over the years, different remediation approaches such as biodegradation (Li and Zhang 2010) photocatalytic removal (Li et al. 2020) (Li et al. 2021), microextraction (Mohebi et al. 2020), ozonation (Andreozzi et al. 2005), electrodegradation (Choudhary et al. 2021), and solid-phase extraction (Opriş et al. 2013) methods have been adopted commonly to manage the pharma wastewater. Among them, biological wastewater treatment is not very effective due to its toxic effects on microorganisms (Chen et al. 2019). The photocatalysis process still has some shortcomings, such as technological restrictions, limited efficiency, and the release of specific pollutants and/or by-products into the environment, etc (Iervolino et al. 2020). In comparison, the adsorption processes using highly porous materials with exceptional surface area have been proven to be more mature, reliable, and environmentally friendly alongside having the capacity to renew and recharge (Rashidi Nodeh and Sereshti 2016) (Pham et al. 2021) (Hassan et al. 2020). Nevertheless, the development of high-capacity and cost-effective adsorbents, which will have a strong affinity towards pharmaceutical wastewater, is yet to appear in the academic and translational paradigms (Rashidi Nodeh and Sereshti 2016) (Sharma et al. 2019). The prior art indicates that many materials such as activated carbon, biomaterials, and nanomaterials have been involved in the adsorption of organic pollutants (Awad et al. 2020). However, the performance of all these materials is still very limited and a high capacity adsorbent is perhaps the need of the hour (Lin and Chang 2015).

In this direction, metal-organic-frameworks (MOFs) are high in demand due to their excellent surface area, porosity, and tailorable structures. MOFs have also emerged as promising materials owing to their large surface area and tunable pore openings (Bhadra et al. 2019). For example, zeolitic imidazolate frameworks (ZIF) have been tipped to be one of the very capable MOF materials with excellent chemical and thermal stability (Park et al. 2006) (Wang et al. 2020a). In general, it is formed by tetrahedral metal ions (Zn, Co, etc.) linked by an imidazolate network (Pan et al. 2011). The ZIFs present a combination of properties of both zeolites and MOFs (Thi et al. 2018). These materials can be significantly stable in an aqueous solution and exhibit excellent adsorption capabilities towards different organic pollutants (Kiwan et al. 2021a) (Kiwan et al. 2021b). Thus, of late, it has been tested in various applications including heterogeneous catalysis and chemical sensing (Lin and Chang 2015). In general, ZIF-67 is formed by linking cobalt moieties with imidazolate anions and arranging them in a sodalite type of topology. Recently, this material has been extensively examined for its adsorptive properties towards the removal of methyl orange, methylene blue, acid blue, malachite green, Cr(VI), 1-naphthol, etc. from the wastewater (Park et al. 2006). Carbonization is a facile way to produce porous nanomaterial embedded in carbon nanostructures generated from MOFs. The large surface area of such materials allows for their use for versatile applications including adsorption (Yang et al. 2019).

In this research article, we aim for an economically viable efficient adsorbent, which utilizes a facile way to remove a wide range of antibiotics with easy separation capabilities. For this purpose, the coral-like Co@Co_3O_4/C hybrids have been synthesized by calcination of pristine MOF produced at room temperature via wet chemical approach. The materials are found to be significantly porous and exhibit excellent magnetic properties. The materials are characterized by X-ray diffraction (XRD), field emission scanning electron microscopy (FESEM), transmission electron microscopy (TEM), Raman spectroscopy, BET surface area measurements, SQUID magnetic study, FTIR, ZETA surface potential study, etc. To judge the performance of this material as an adsorbent, we have chosen three different classes of antibiotics such as nalidixic acid (NAL) and ciprofloxacin (CIP) from the quinolone group, tetracycline (TC) from the tetracycline group, and sulfamethoxazole (SMX) belonging to sulfonamide group, respectively. The as-synthesized material shows excellent adsorption efficiency against all the different classes of antibiotics chosen. Different reaction parameters for adsorption experiments, such as time, pH, and amount of adsorbent, have been assessed to study the behaviour of the adsorbents. Further, the superior magnetic properties of this material enable a facile separation of them after the adsorption of the antibiotics on their surface and pores. Finally, the Co@Co_3O_4/C hybrids show excellent recyclability as demonstrated by the four cycled adsorption squeezing process. The novelty of the research lies in utilization of a cost-effective pH dependent adsorbent against a variety of antibiotics as well as its ease of separation using an external magnet.

Materials and methods

The precursors for the synthesis of adsorbents and adsorption experiments were of analytical grade and used without any further purification. Cobalt nitrate $Co(NO_3)_2.6H_2O$ (98%) and 2 methyl imidazole ($C_4H_6N_2$) (98%) were purchased from Sigma Aldrich. Nalidixic acid (≥ 98%) tetracycline (≥95%), sulfamethoxazole (analytical standard), and ciprofloxacin (98%) were obtained from Sigma Aldrich. Methanol has been procured from Merck, India.

Synthesis of ZIF-67 crystal

In a typical experiment, 15 mmol of $Co(NO_3)_2.6H_2O$ was dissolved in 50 ml methanol. The preceding solution was gradually added to 25 mmol of 2-methylimidazole solution. The resultant solution became dark violet. The mixture was then stirred overnight at room temperature. Further, the sample was collected by centrifugation followed by rinsing with methanol repeatedly until unwanted residues were removed. Finally, the resultant sample was dried at 60 °C overnight to get the final product ZIF-67.

Synthesis of coral like $Co@Co_3O_4/C$

The as-synthesized ZIF-67 sample was calcined at 700 °C under nitrogen environment for 4 h. After cooling down to room temperature, a black colour sample was collected. Subsequently, these calcined sample was characterized in detail by different techniques.

Characterization of adsorbent

XRD spectra were obtained by a Rigaku Smart Lab (9) diffractometer with Cu Kα radiation ($\lambda = 1.5406$ Å) from 5 to 90°. Field emission scanning electron microscopy (FESEM) and energy-dispersive spectrometer (EDS) maps were acquired with JEOL-JSM-7800F. The detailed study of the morphology was carried out by high-resolution transmission electron microscopy (HRTEM, JEOL-JEM-2100F). The surface area and pore size analysis of the adsorbents were done by N_2 adsorption on a Quantachrome AUTO-SORB-IQ-MP surface area and pore size analyser and high-pressure surface analyser at 77 K. The sample was degassed at 300 °C for 2 h prior to the BET measurements. The room temperature Raman spectra was recorded by Renishaw via a Raman spectrometric analyser equipped with an Ar^+ ion laser having a laser power of 2.5 mW (excitation source with 514.5 nm line). The resolution of the Raman spectra was ~0.5 cm^{-1}. X-ray photoelectron spectroscopy (XPS) measurements were performed by using PHI 5000 Versa Probe III. The adsorption studies were validated by UV-Vis spectrometer (Shimadzu UV-2600) in the range of 200–700 nm at room temperature. Adsorbents had some distinctive magnetic properties, which were estimated by Mpms XL 7 SQUID magnetometer at room temperature in the range of −7 to 7 T. Moreover, the FTIR spectra were recorded by NICOLET-IS-50. RP-HPLC studies was acquired on Agilent 1260 Infinity using a C18 column (150 mm × 4.6mm × 5 µm). ZETA surface potential measurements were performed using RDET 48125 Zetasizer Nano ZS (Malvern).

Adsorption experiments

A calibration curve was plotted for NAL with a series of standard solutions (0.1–100 mg/L) obtained from diluting the stock solution. Subsequently, the initial and equilibrium concentrations of NAL were measured using a calibration curve. The coral-like $Co@Co_3O_4/C$ hybrids were used as the adsorbent for an aqueous solution at 303 K (room temperature). Moreover, 40 mg of samples were added to the aqueous solution of antibiotics. Afterwards, the mixture was shaken in a room temperature shaker at 120–130 rpm for 5–120 min. No magnetic stirrer was needed as the adsorbent material showed excellent magnetic properties. The aliquot solution was collected by an external magnetic field after certain time intervals. The supernatant solution is further analysed by a UV–Vis spectrometer in the wavelength range of 200–800 nm. The same procedure was followed for other three antibiotics as well. The influence of pH on the adsorption of antibiotics was measured by adjusting the pH values in acidic and basic ranges. Additionally, the adjustment of pH values was accomplished using 0.1 mol L^{-1} HCl and 0.1 mol L^{-1} NaOH solutions. The adsorption capacity (q_e) was calculated by the following (Eq. 1),

$$q_e = \left(C_0 - C_e\right) \times \frac{V}{m} \tag{1}$$

where the C_0 and C_e were the initial and equilibrium concentration of NAL, respectively. Additionally, V (L) represents the volume of the NAL aqueous solution, and m (g) was the mass of the $Co@Co_3O_4/C$ adsorbent. The pH of the solution was varied from pH 3 to 12. The adsorption capacity was measured for coral-like $Co@Co_3O_4/C$ hybrids using Eq. 1. Moreover, the experimental adsorption data were fitted in different adsorption kinetics accordingly.

The reusability of the adsorbent was checked by collecting the adsorbent after adsorption and rinsing it in ethanol and water solution. For this purpose, a 40 mg of the adsorbent was placed into 50 ml of ethanol and sonicated for 15 min followed by the same process in water. Subsequently, the material was collected and dried at 60 °C. This procedure was repeated 3–4 times

to remove the adsorbed antibiotic molecules completely. Then, the regenerated adsorbent was utilized for antibiotics adsorption for up to four cycles.

Selective adsorption experiments

The selective adsorption experiments for the adsorbent were accomplished by making one simulated pharmaceutical wastewater with four different antibiotics: NAL, CIP, TC, and SMX. The concentration of each antibiotic was kept constant at 15 mg/L. Adsorbent (40 mg) was introduced to a 20-mL mixed solution before the adsorption. The solution pH was maintained at pH 6. The suspension was kept on a shaker at 130 rpm for 10 min, and aliquots were withdrawn at specific time intervals. To test the selectivity, the aliquot solution was investigated by RP-HPLC analysis. Final concentration of each antibiotic in the simulated solution was calculated from the RP-HPLC analysed data. The detailed procedure of RP-HPLC was given in supporting data.

Results and discussion

Detailed characterization

The synthesis procedure is depicted in Scheme 1. The crystallization of ZIF-67 crystals happens during the room temperature stirring of precursors. In this research work, we have adopted a wet chemical approach to synthesize ZIF-67 crystals, in which 2-methylimidazole diffuses into the system and interacts with Co^{2+} ions. However, the solution colour is changed to dark violet as a result, allowing for the nucleation and subsequent development of ZIF-67 crystals. The polyhedral framework, on the other hand, collapses during pyrolysis, resulting in uniform porosity structures. The phase purity and composition of the synthesized samples are determined by comparison of the XRD spectra with the simulated XRD data of pure ZIF-67 crystal.

The detailed XRD spectra in Fig. 1a reveals presence of prominent peaks at 2θ = 7.32°, 10.44°, 12.78°, 14.74°,

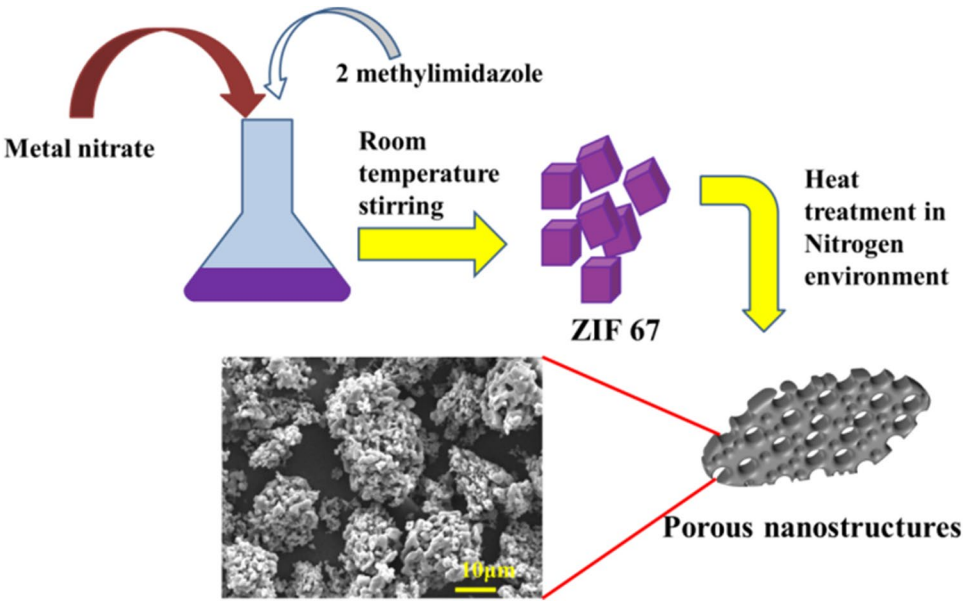

Scheme 1 Synthesis scheme of coral-like Co@Co_3O_4/C nanohybrids

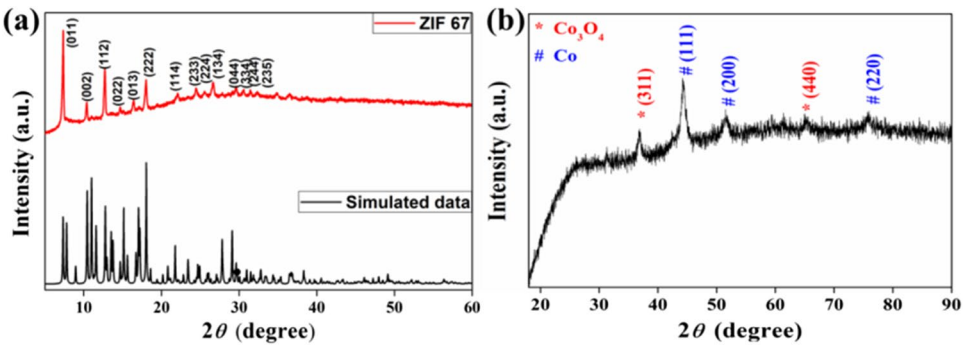

Fig. 1 **a** XRD spectra of ZIF-67 crystal. **b** Detailed XRD spectra of heat-treated ZIF-67 sample

16.34°, 18.05°, 22.07°, 24.49°, 25.56°, 26.64°, 29.67°, 30.57°, 31.38°, and 32.36° corresponding to the (011), (002), (112), (022), (013), (222), (114), (233), (224), (134), (044), (334), (244), and (235) planes, respectively, of pure ZIF-67 crystals (Guo et al. 2016). Figure 1 b shows the XRD spectra for the material after pyrolysis. There are three distinctive peaks at $2\theta = 44.29°$, 51.50°, and 75.96° corresponding to (111), (200), and (220) lattice planes of metallic Co nanoparticles (Li et al. 2016). A broad peak at $2\theta = 25.88°$ in the XRD plot corresponds to the characteristic (002) peak of carbon. At the same time, another two low-intensity peaks at 36.82° and 65.03° represents (311) and (440) lattice planes of Co_3O_4 nanoparticles (El Bachiri et al. 2018).

The morphology of the ZIF-67 crystals and porous Co@Co_3O_4/C nanohybrids are analysed using FESEM and HRTEM images. Figure S1 reveals that the ZIF-67 synthesized at room temperature possess an uniform polyhedron structure with smooth faces and sharp edges. The approximate size of the polyhedron-like structure is 1.5–2.0 µm. Moreover, the FESEM images of the Co@Co_3O_4/C nanohybrids in Fig. 2 a–d confirm uniform porous coral-like structures. The polyhedron structure collapses when ZIF-67 crystals are pyrolysed in a controlled N_2 environment, resulting in the porous Co@Co_3O_4/C structure. The energy-dispersive X-ray spectroscopy (EDS) elemental mapping in Fig. S2 confirms the uniform elemental distribution of C, N, O, and Co throughout the porous structures. The atomic percentage of cobalt is obtained to be more than other elements and the excess cobalt can further be reduced to form Co nanoparticles (Chen et al. 2018). The pristine MOF crystal is converted to metal-embedded porous carbon network after carbonization. However, no additional carbon source is introduced for the proposed synthesis process. The coral-shaped Co@Co_3O_4/C hybrid networks are obtained to be extremely porous and could further protect other metal particles from aggregation. The high-resolution TEM images that are depicted in Fig. 2 e–f reveal the presence of tubular structures in Co@Co_3O_4/C corals.

Moreover, there are three types of lattice fringes in the HRTEM image. Firstly, 0.207 nm and 0.143 nm lattice spacing corresponds to the cobalt (200) plane and Co_3O_4 (440) planes, respectively (Duraisamy et al. 2017). The interplanar spacing at 0.34 nm in the porous sample represents the

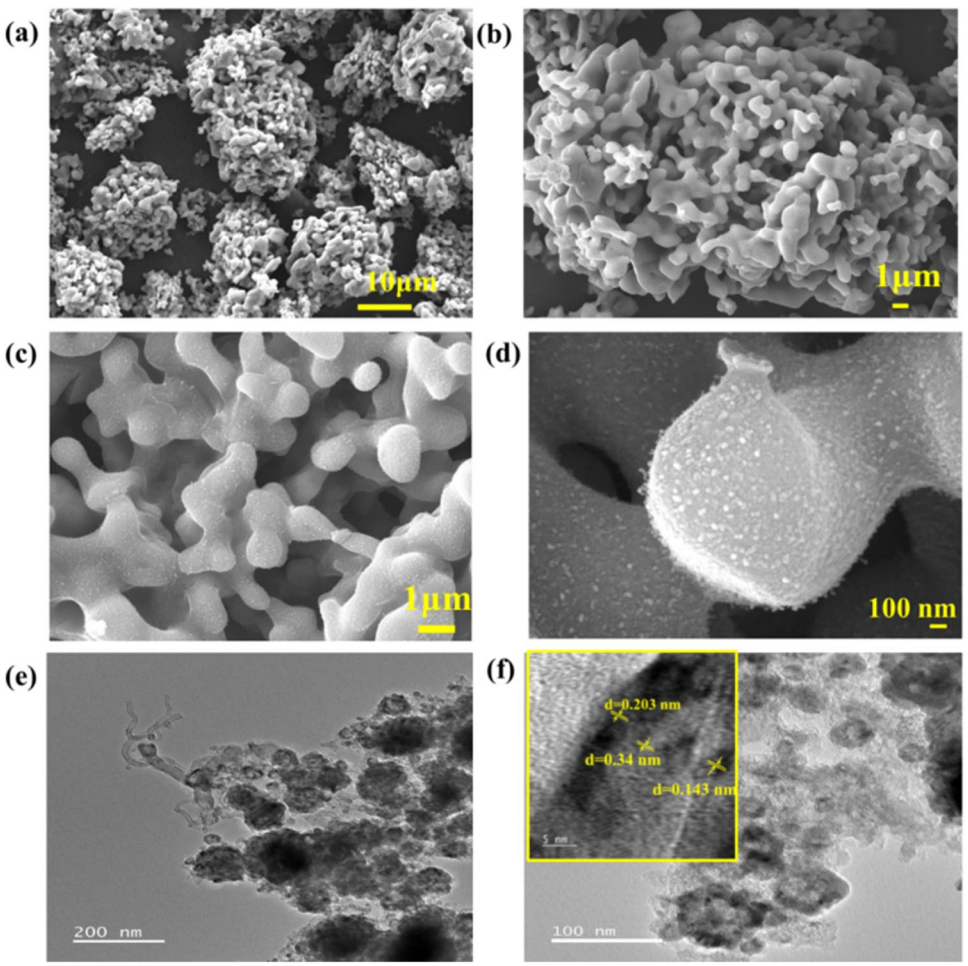

Fig. 2 **a**, **b**, **c**, **d** FESEM images of Co@Co_3O_4/C adsorbent. **e**, **f** TEM image of the adsorbent with lattice image in the inset

presence of graphitic carbon (Wu et al. 2019). Nevertheless, the simultaneous presence of multivalent cobalt is further supported by the XRD spectra.

The chemical composition analysis and elemental valence states of Co@Co_3O_4/C adsorbent are studied using XPS analysis (Fig. 3a–d). Firstly, the survey XPS spectra (Fig. 4a) reveal the presence of intense peaks corresponding to Co 2p, C 1s, O 1s, and N 1s XPS, respectively. Additionally, there are some low-intensity peaks of Co 3s and Co 3p orbital. The high-resolution C 1s spectra depicts two distinctive peaks at about 284.8 and 287.6 eV ascribing to C-C and C-O bonds, respectively (Chen et al. 2018). The deconvolution of N 1s peaks can be indexed to pyridinic-N (398.7 eV), pyrrolic-N (400.01 eV), and graphitic-N (401.7 eV). The meticulous deconvolution of Co 2p spectra leads to the occurrence of seven peaks in total. The Co $2p_{3/2}$ core level spectrum can be fitted with four components corresponding to Co^0, Co^{2+},Co^{3+}, and satellite peaks. The Co^{2+} $2p_{3/2}$ and $Co^{2+}2p_{1/2}$ peaks are situated at 781.8 eV and 799.6 eV, respectively. Similarly, the peaks at 780.6 eV and 795.7 eV are ascribed for Co^{3+} $2p_{3/2}$ and $Co^{3+}2p_{1/2}$, respectively. Furthermore, there are some other peaks at 779.56 eV and 789.03 eV corresponding to the metallic cobalt (Co^0) (Chen et al. 2018) (Wang et al. 2020c). The presence of +3, +2, and mental states of cobalt concurrently indicate the coexistence of Co_3O_4 and metallic cobalt.

Micro-Raman spectra in Fig. 3e reveals two distinctive peaks at 1341 and 1595 cm^{-1} corresponding to the characteristics D and G band of graphitic carbon. The G band arises from the first-order scattering effect of the E_{2g} phonon sp^2 carbon atoms and indicates the formation of graphitic carbon (Wang et al. 2014). Additionally, the D band in Raman spectra describes the breathing mode of κ point phonons of A_{1g} symmetry. Additionally, the relative

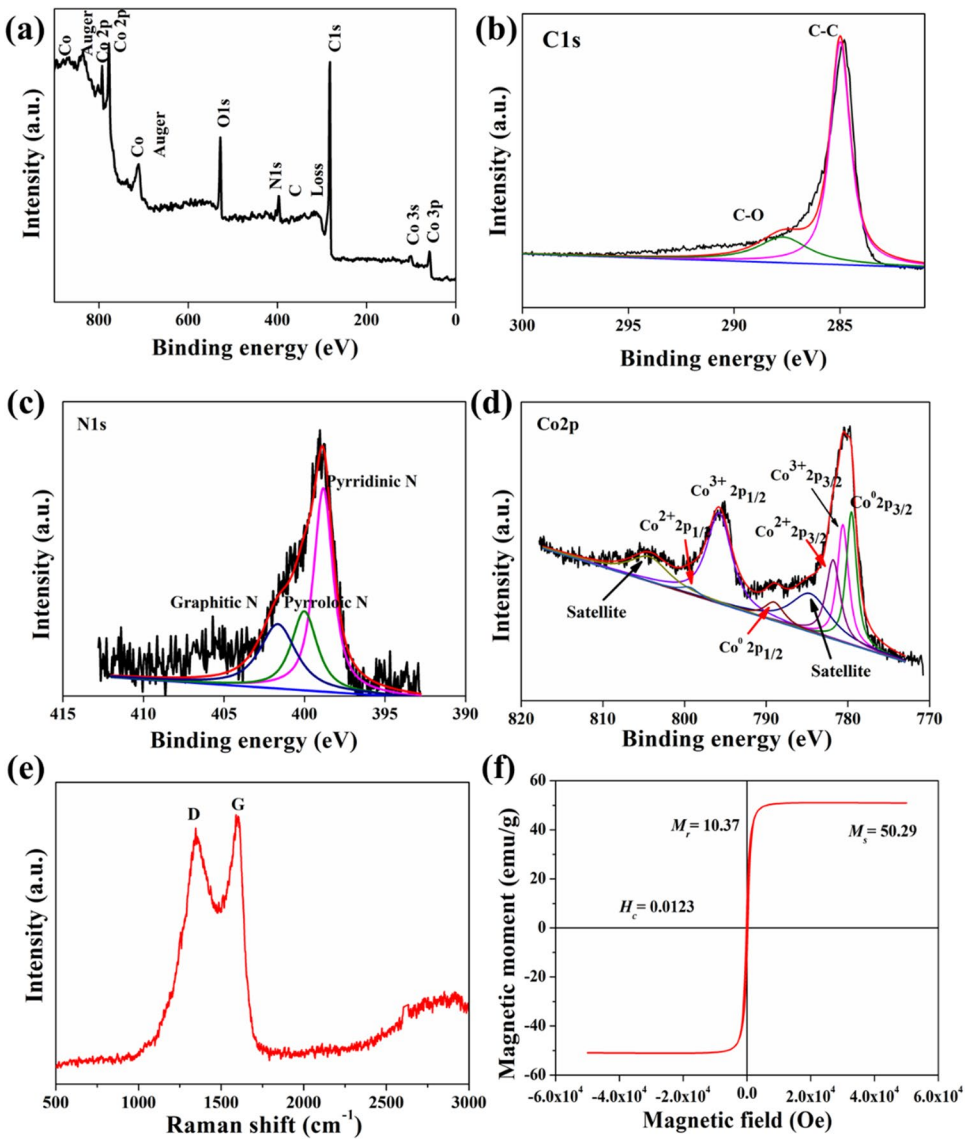

Fig. 3 X-ray photoelectron spectroscopy (XPS) spectra of Co@Co_3O_4/C hybrids: **a** survey spectra, **b** C1s spectra, **c** N1s spectra, **d** Co 2p spectra, and **e** micro-Raman spectra of Co@Co_3O_4/C adsorbent. **f** Squid analysis of Co@Co_3O_4/C adsorbent at room temperature

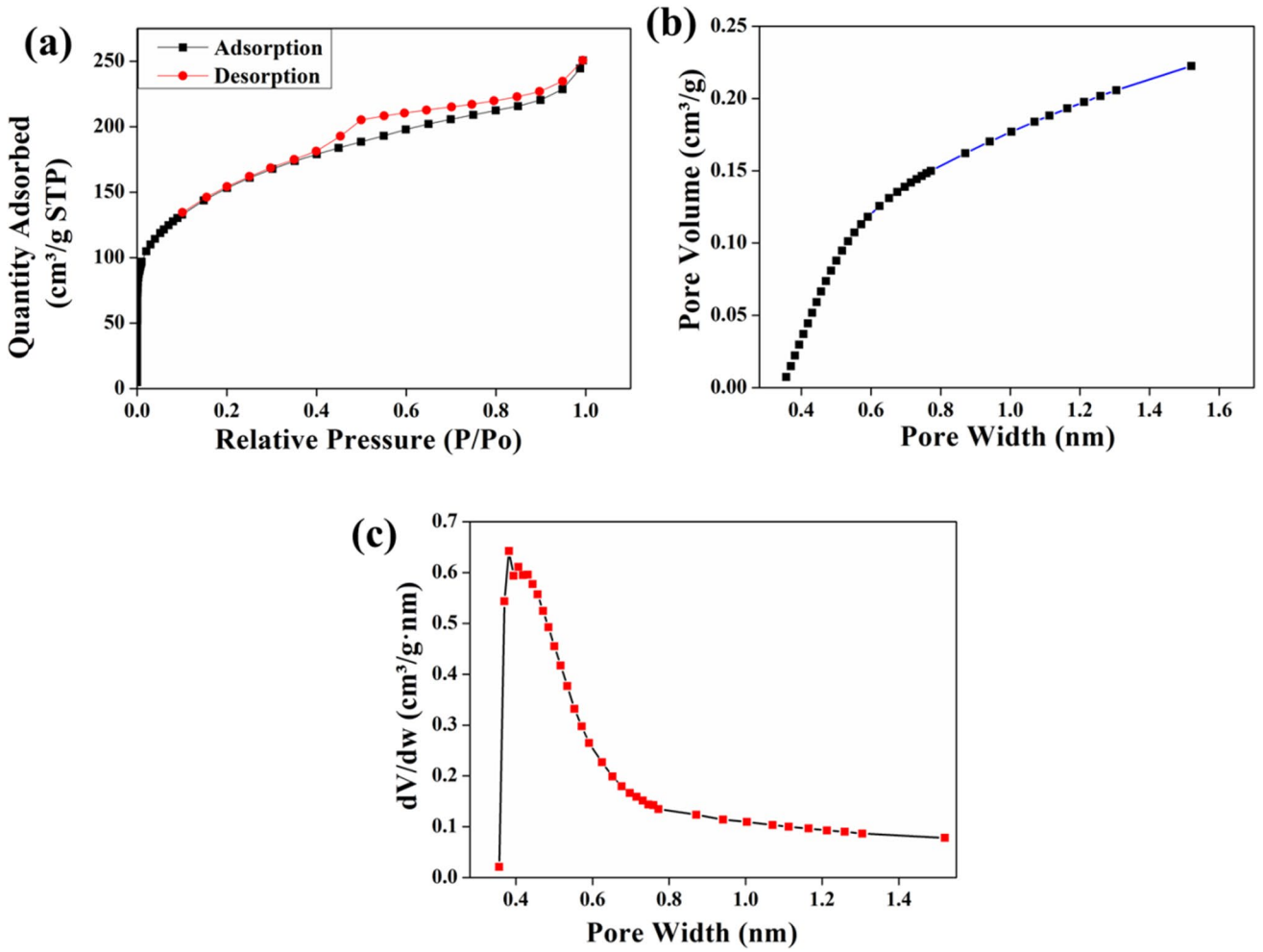

Fig. 4 **a** N_2 adsorption/desorption isotherms, **b** pore volume distribution, and **c** pore size distribution as dV/dw vs. pore width graph (where *V* is the pore volume and effective pore width)

ratio of the two characteristic bands provides information about the crystalline degree of graphitic carbon (Suhag et al. 2015) (Li et al. 2017). The band intensity ratio of the D and G bands (I_D/I_G) is a widely used phenomenon for determining the degree of defects in carbon (Gao et al. 2022). The $I_G/I_D = 1.09$ value is calculated from Fig. 3e indicating well-developed graphitic structures in the material supporting the TEM lattice image.

Squid analysis is used to demonstrate the magnetic characteristics of the material. The static hysteresis loop (Fig. 3f) of the Co@Co_3O_4/C material has been recorded, and the result is significantly reliant on the state of cobalt in the structure. Moreover, the saturation magnetization, coercive field, and remanence magnetization of the material are measured to analyse its magnetic response at room temperature. The magnetic observation depicts a significantly high value of saturation magnetization (M_s) at room temperature equal to 50.29 emu/g. The corresponding values of the coercive field, as well as remanence magnetizations, are 0.0123 Oe and 10.37 emu/g, respectively. The information that has been extracted from the magnetic study signifies the occurrence of a ferrimagnetic type of behaviour in the material. However, the low value of a coercive field of the sample may be attributed to the existence of large dispersion of particles in the materials. Further, the low coercive field of the sample at room temperature exhibits the behaviour which is the typical fingerprint of magnetic nanoparticles in the superparamagnetic regime (Garbarino et al. 2013). The magnetic property of porous Co@Co_3O_4/C nanohybrids can be attributed to the metallic cobalt nanoparticles present in the system and uncompensated surface spins of Co_3O_4 derived from ZIF-67.

The surface area of the synthesized adsorbent is studied by using the nitrogen adsorption and desorption isotherms as shown in Fig. 4. The specific surface area of the sample is evaluated to be 554.8 $m^2\ g^{-1}$ with a maximum pore volume of 0.22 cm^3/g. Moreover, BET studies depict mean pore diameter

of 2.79 nm. This excellent surface area of the adsorbent from BET measurement in correlation with excellent coral-like porous structure from FESEM images leads to the excellent adsorption performance towards a range of antibiotics.

Adsorption — behaviour, time, dosage, and loading

The adsorption behaviour of coral like Co@Co_3O_4/C hybrids is examined in Fig. 6 for NAL at room temperature. Moreover, the influence of different reaction parameters on the adsorption characteristics of the adsorbent is also observed. Figure S3 depicts the comparison of removal efficiency between pristine MOF and coral-like Co@Co_3O_4/C hybrids for NAL. It shows that pristine MOF is unable to show notable efficiency against the antibiotics. There is a substantial increase in the adsorption efficiency after heat treatment of the MOF which further specify the role of carbon network in the adsorbent material.

A detailed adsorption study for 24 h (Fig. 5a) has been carried out to study the effect of contact time on the NAL adsorption by the Co@Co_3O_4/C adsorbent. Initially, the change in NAL concentration over time is used to estimate the adsorption equilibrium time. Although, after 120 min, there is no further change in the final concentration of the NAL implicating that the adsorption equilibrium is attained. The adsorption behaviour of the material for three different concentrations such as 15, 30, and 100 mg L^{-1} is depicted in Fig. 5c. The efficiency of the material lies in terms of using only 40 mg of the Co@Co_3O_4/C adsorbent for the removal process. The adsorption behaviour clearly describes the faster removal process as above 80% removal can be achieved in 30 min only resulting in complete removal of NAL within 120 min.

Adsorbent to adsorbate ratio can significantly influence the overall efficiency of an adsorption process. Therefore, optimization of the adsorbent dosage is very necessary. Figure 5 b describes the effect of adsorbent dosage on the

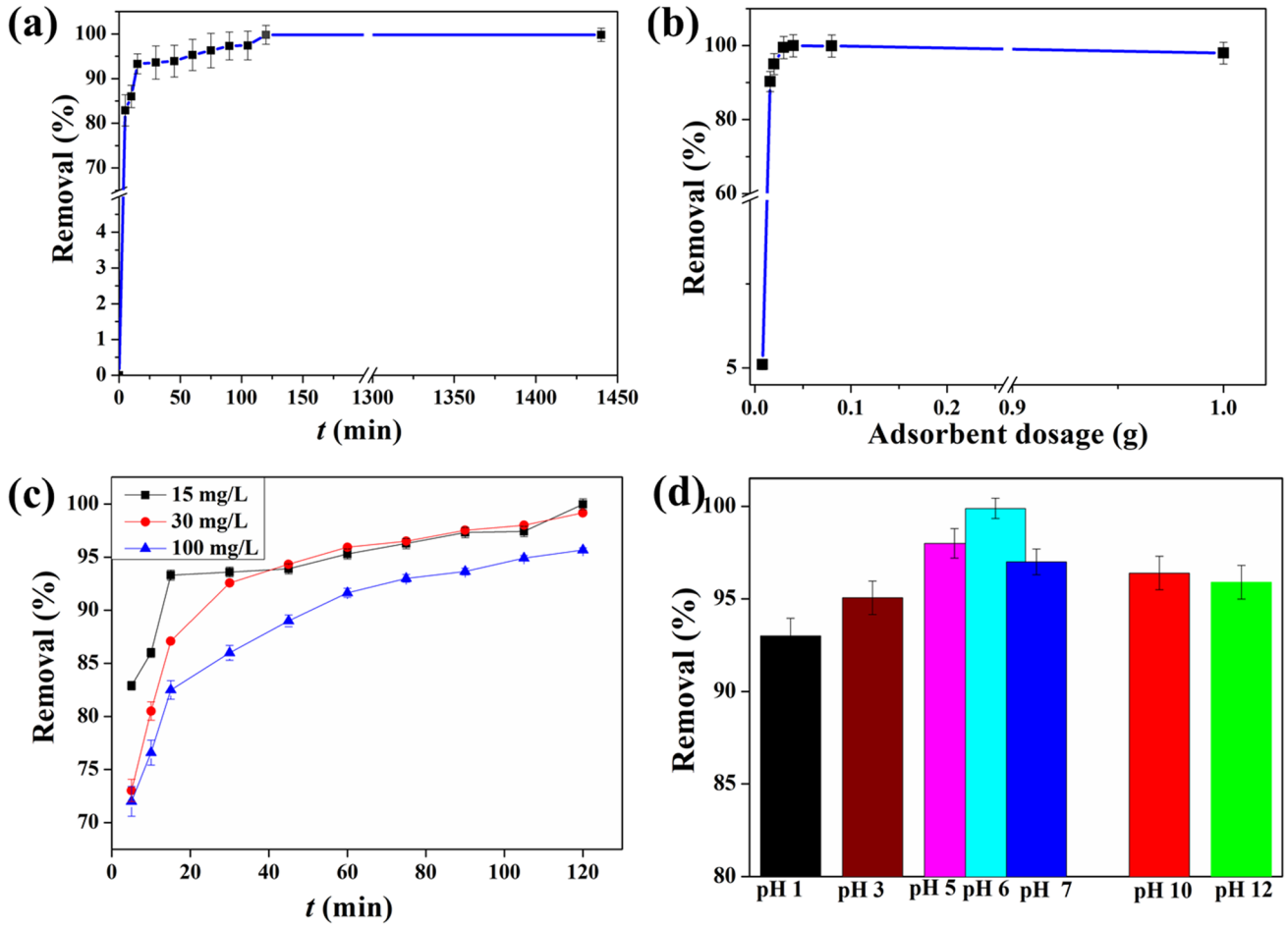

Fig. 5 **a** Effect of contact time on adsorption efficiency for 15 mg/L initial concentration of NAL. **b** Effect of adsorbent dosage on NAL removal by Co@Co_3O_4/C adsorbents. **c** Effect of three initial NAL concentrations on removal efficiency by Co@Co_3O_4/C adsorbents. **d** Effect of pH on removal efficiency of Co@Co_3O_4/C adsorbents. Error bars represent the standard deviation of the mean of three experiments

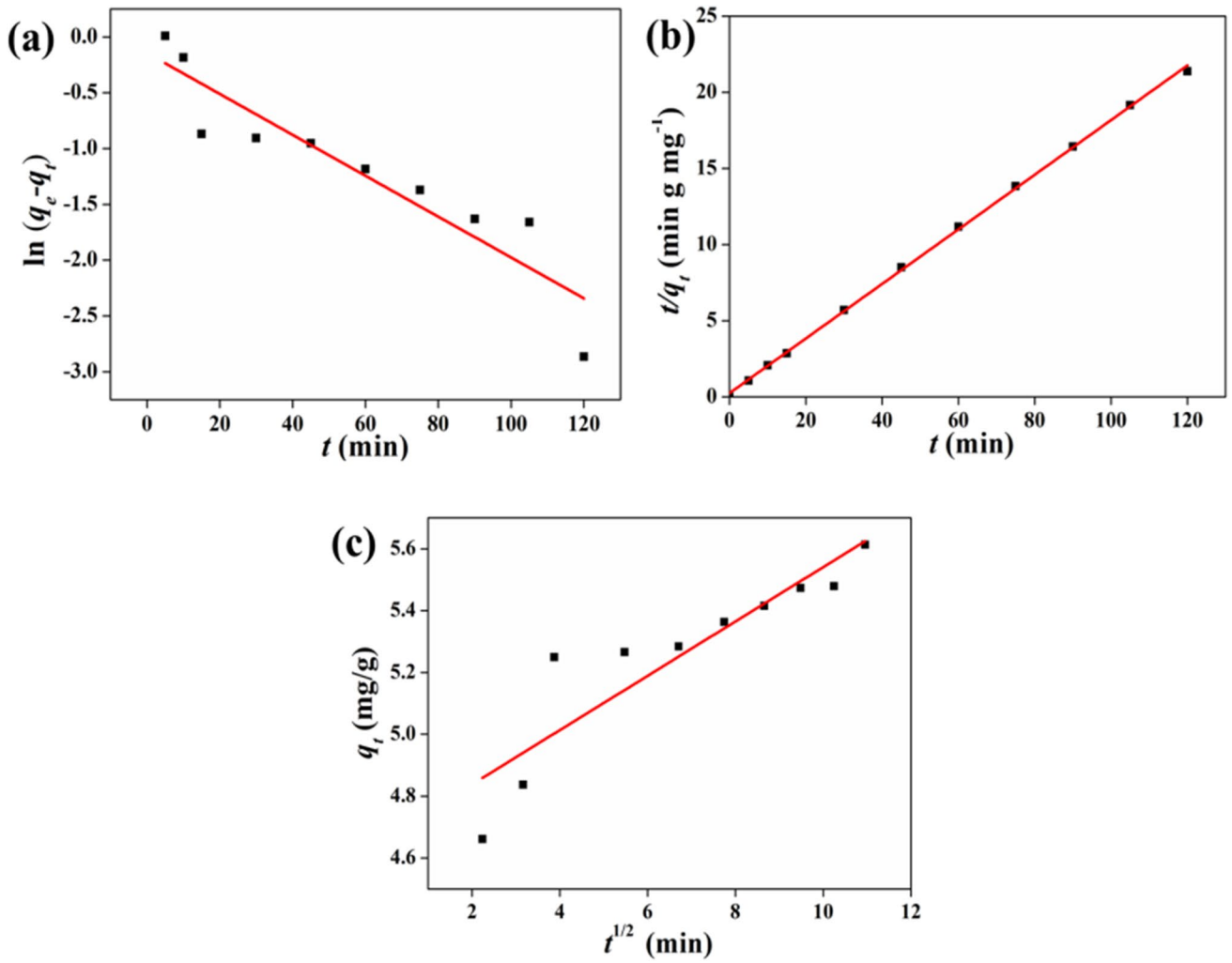

Fig. 6 **a** Pseudo-first-order and **b** pseudo-second-order kinetics fitted data for Co@Co_3O_4/C adsorbents. **c** Intraparticle diffusion spectra of Co@Co_3O_4/C adsorbent

removal efficiency. Seven different adsorbent dosages (8 mg, 16 mg, 20 mg, 30 mg, 40 mg, 80 mg, and 1 g) have been considered for the experiment. The removal efficiency is found to increase with the increase in the adsorbent dosage keeping other reaction parameters constant. The removal efficiency for the adsorbent initially increases to its maximum value before sudden decrease as we continue to increase the adsorbent dosage. The optimum adsorbent dosage is found to be 40 mg, as beyond that that there is no further removal of antibiotics. This correlates to the saturation of the number of active sites for adsorption.

One of the main influencing factors in adsorption is the initial antibiotic concentration. The effect of initial antibiotics concentration on adsorption by Co@Co_3O_4/C is described in Fig. 5c. Subsequently, three concentrations are taken as 15 mg/L, 30 mg/L, and 100 mg/L, respectively, keeping other parameters constant to recognize the effect of initial concentration of NAL. In Fig. 5c, the nature of the curve reveals that at a given time, the removal percentage decreases as we increase the initial concentration due to a fixed number of adsorption sites (Senthil Kumar et al. 2010). The present data indicate that Co@Co_3O_4/C material can efficiently act as an excellent adsorbent for a wide range of initial antibiotic concentrations.

Effect of pH on removal efficiency

The effect of solution pH is also monitored by keeping other reaction parameters constant. The removal efficiency of NAL gradually increases with rising pH value and attains a maxima at pH 6, as shown in Fig. 5d. This phenomenon can be attributed to the electrostatic interaction between NAL and Co@Co_3O_4/C material. NAL (pK_a value of 5.95) exists predominantly as neutral species at lower pH, whereas the anionic form prevails above pH 5.95 (Wu et al. 2013). Zeta potential measurements of Co@Co_3O_4/C at different pH

confirm its isoelectric point (pH_{iso}) at pH 6.33 (Fig. S4). Consequently, positive charge is developed on the adsorbent surface at pH < pH_{iso} leading to the highest adsorption efficiency at pH 6. Moreover, at pH > pH_{iso}, the reduction in adsorption efficiency is due to the development of negative charges on the surface of the adsorbent triggering electrostatic repulsion between adsorbent surface and anionic NAL species. However, the adsorption of NAL at higher pH predominantly is dominated by π–π interactions between the aromatic rings of NAL molecules and the π-electron network of the graphitic carbon present in the Co@Co_3O_4/C adsorbent (Peng et al. 2016).

Adsorption kinetics and isotherm

The nature of the adsorption process is assessed by adapting pseudo-first-order and pseudo-second-order kinetic models to the adsorption data. The adsorption capacity increases by raising the initial concentration of the NAL molecules which in turn indicates the abundance of adsorption sites on the Co@Co_3O_4/C surface. Subsequently, the adsorption increases with the increase in contact time indicating a probable decrease in boundary layer resistance to mass transfer in the solution (Senthil Kumar et al. 2010). In this regard, the pseudo-first-order and pseudo-second-order model is given by

$$q_t = q_e\left(1 - k_1 t\right) \tag{2}$$

$$\frac{1}{q_t} = \frac{1}{k_2 q_e^2} + \frac{t}{q_e} \tag{3}$$

where q_e and q_t (mg/g) is the mass of the antibiotics adsorbed per unit mass of the Co@Co_3O_4/C adsorbent at equilibrium at time t (min), respectively. Further, k_1 (1/h) and k_2 (g/mg/h) are the rate constants of the first-order and second-order kinetic models. The adsorption data of Co@Co_3O_4/C adsorbent for NAL at 15 mg/L concentration is fitted through the kinetics model and shown in Fig. 6 a and b. Table S1 shows the calculated values of rate constants and q_e (mg/g) for both pseudo-first-order and pseudo-second-order kinetic models are fitted to the practical adsorption data. The adsorption data for Co@Co_3O_4/C adsorbents is found to be best fitted with the pseudo-second-order model (R^2~0.99936) than the pseudo-first-order (R^2~0.84447) one.

The adsorption data is also fitted in the intraparticle diffusion model, which is defined by the following equation,

$$q_t = K_d\sqrt{t} + C. \tag{4}$$

Here, K_d signifies the intraparticle diffusion rate constant and can be calculated by the slope of the q_t vs $t^{1/2}$ plot. And C is the boundary layer thickness given by the intercept of q_t vs $t^{1/2}$ plot. If the plot is linear and goes through the origin, then we can consider intraparticle diffusion as a slow step process. Figure 6 c denotes the intraparticle diffusion model fitted to the experimental adsorption data, and Table S4 shows the value of $C \neq 0$ indicating the presence of some degree of boundary layer control.

The parameters of different adsorption kinetics reveal that experimental data have the best fit with the pseudo-second-order kinetics model ($R^2 = 0.99936$) where the adsorption is dependent on both adsorbents and adsorbate. The pseudo-second-order kinetic model further indicates chemical adsorption involves electrostatic force of attraction during the adsorption processes.

The adsorption data has been fitted to the Langmuir and Freundlich models. The equation for Langmuir and Freundlich isotherm models are given by the following equation.

$$q_e = \frac{Q_m K_L C_e}{1 + K_L C_e} \tag{5}$$

$$q_e = K_F C_e^{1/n} \tag{6}$$

There is a dimensionless constant separation factor (R_L) for Langmuir isotherm which is defined by,

$$R_L = \frac{1}{1 + K_L C_0} \tag{7}$$

Here, C_e and C_0 denote equilibrium and the highest initial concentration of antibiotics. q_e (mg/g) is the equilibrium adsorption capacity. And, K_L (L mg^{-1}) and K_F (mg g^{-1} (mg $L^{-1})^{-1/n}$) represent the adsorption rate constants of Langmuir and Freundlich models, respectively. The calculated R_L value (dimensionless Langmuir separation factor) gives an idea of the properties of the adsorption process.

$R_L = 0$ represents reversible process

$0 < R_L < 1$ represents a favourable process

$R_L > 0$ represents an unfavourable process

The adsorption data of Co@Co_3O_4/C adsorbent for NAL is fitted through both Langmuir and Freundlich isotherm models. The parameters of the two isothermal models are compared using the equilibrium data. Here, the nonlinear regression model is adapted for the adsorption data. The fitted data for two adsorption models are depicted in Fig. 7. The experimental adsorption data is fitted better with the Langmuir model ($R^2 = 0.9922$) signifying homogeneous and monolayer adsorption. However, the maximum adsorption capacity is obtained at 38.61 mg/g, which matches well with the experimental data ${q_m}^{exp} = 35.87$ mg/g. Table S5 indicates the calculated value of R_L to be 0.005 which is in the range of 0 to 1 referring to the adsorption process being favourable. That means the antibiotics could easily adsorb

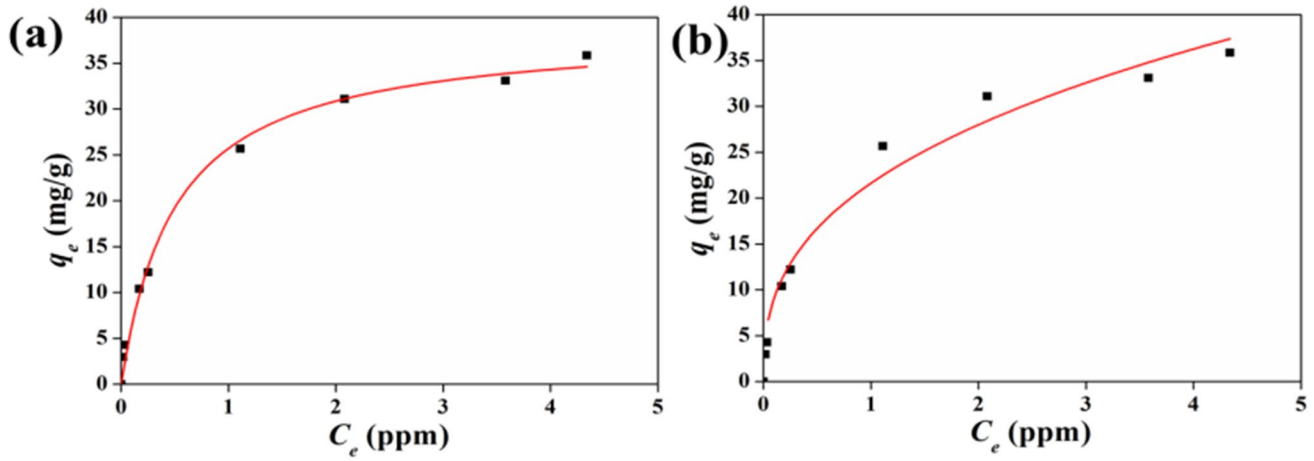

Fig. 7 **a** Langmuir isotherm model and **b** Freundlich isotherm model for NAL adsorption of Co@Co_3O_4/C adsorbents

on the adsorbent surfaces. On the contrary, the 1/*n* value from the Freundlich model is found to be ~0.37, which is between 0 to 0.5 indicating an easy adsorption process (Wang et al. 2020b). These isotherm data are found to be consistent with the excellent adsorption efficiency of the material towards antibiotics.

Interference studies — effect of coexisting ions

Exogenous ions in wastewater compete fiercely with NAL molecules for adsorption sites in the adsorbent. In this work, the effect of three anions and three cations are examined to assess the influence of different interfering ions in wastewater. Figure 8 reveals the influence of coexisting cations and anions on the adsorption efficiency of the adsorbent. The concentration of the NAL has kept at 15 mg/L in each case.

The presence of Zn^{2+}, Cd^{2+}, and Fe^{2+} cations has an inconspicuous effect on adsorption efficiency compared to the efficiency in the absence of any co-existing ions. Zeta surface charge studies articulate that the surface of the adsorbent is positively charged which electrostatically attract the anionic antibiotic molecules and repel the positively charged coexisting metal cations. Conversely, there is a slight decrease in the adsorption efficiency which can be attributed to ion permeation into the adsorbent surface further increasing the adsorbent particle aggregation.

Additionally, at high salt concentration, ions may compete with antibiotic molecules for an effective binding site on the exterior surface of the adsorbent. Contrariwise, the

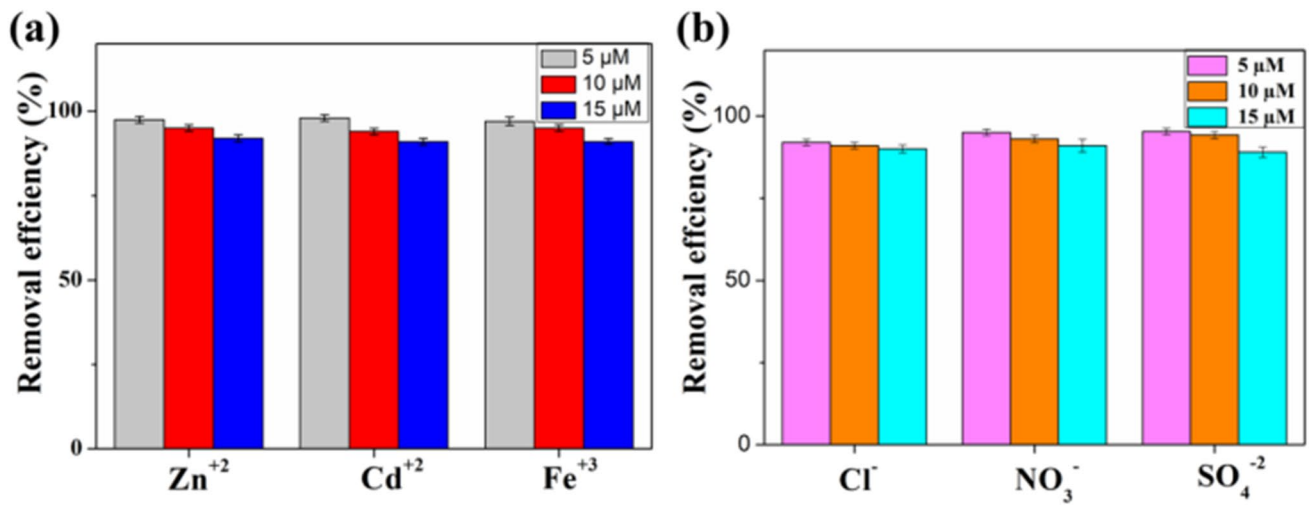

Fig. 8 Effect of coexisting **a** cations on removal efficiency Co@Co_3O_4/C adsorbents and **b** anions on removal efficiency of NAL by Co@Co_3O_4/C adsorbents. Error bars represent the standard deviation of the mean of three experiments

present study also examines the effect of anions (Cl^-, NO_3^-, SO_4^{2-}) on the adsorption of antibiotics. There is an inhibition in the adsorption efficiency with a gradual increase of competitive anion concentration from 5 to 15 mmol. The effects of anions are expected to be significant due to electrostatic attractions with the positive adsorbent surface. The anionic antibiotic molecules compete with the coexisting anions for effective adsorption sites on the Co@Co_3O_4/C adsorbent, thus inevitably compromising the rate of diffusion to the surface of the adsorbent and finally decreasing the adsorption efficiency.

FTIR measurement further confirms the chemisorption nature of the NAL adsorption by the Co@Co_3O_4/C nanohybrid. Figure 9 signifies the changes in the functional groups in the Co@Co_3O_4/C adsorbent before and after the adsorption. The nature of the two spectra matches well except there is a distinctive change in intensities of some of the bonds present in the material. A sharp peak at 3416 cm^{-1} may be attributed to the stretching vibration of hydroxyl and amino groups. Further, there is a sudden increase in the intensity of this particular bond after adsorption. This phenomenon can be explained by the possible interaction between adsorbents and NAL molecules (Du et al. 2017). A small peak at around 575 cm^{-1} indicates the Co-O stretching vibration (Shahabuddin et al. 2016). Another two peaks at 837 cm^{-1} and 2920 cm^{-1} are ascribed to C-H and asymmetrical CH_2 stretching, respectively (Hedrick and Chuang 1998). There is a slight decline in the intensity of the two bonds, which may be due to the interaction between adsorbate and Co@Co_3O_4/C adsorbents. There are some other additional peaks such as 1620 cm^{-1} indicating C = C characteristics vibration and peak position at 1400 cm^{-1} for COO stretching vibrations (Nazari et al. 2016). There is an increase in bond intensity of C = C bond at 1620 cm^{-1} after adsorption attributing to the π−π interaction which further indicates the interaction

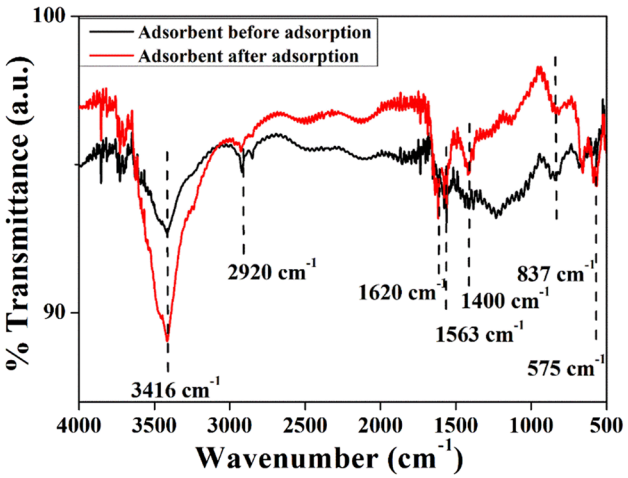

Fig. 9 FTIR spectra of adsorbent before and after adsorption of NAL

between the aromatic π-electron clouds of NAL and the graphitic carbon present in the carbon network of Co@Co_3O_4/C (Huang et al. 2020) (Peng et al. 2016).

The binding energies of all elements before and after the antibiotic adsorption are shown in Fig. S4. The deconvoluted spectra of cobalt remains unchanged in the post adsorption indicating no change in the oxidation states of Co after adsorption. The overall structure remains unchanged with potential surface modifications. There is substantial peak shift for carbon indicating the potential π–π interaction between the adsorbent surface and antibiotic molecules. Additionally, a peak shift in oxygen molecule XPS spectra also indicates the dominant adsorption by surface oxygen and carbon bonds. However, there was no change observed in chemical valency of the adsorbent elements before and after the adsorption process indicating the involvement of any redox process. This data is further supported by FTIR analysis. (Li et al. 2019)

Adsorption mechanism

This recent research specifies that there are multiple mechanisms coexist in the system, such an electrostatic interaction, π–π interactions, hydrogen bonding and hydrophobic effect. The adsorbent Co@Co_3O_4/C is a metal-embedded carbon, synthesized from the MOFs having excellent adsorption properties towards NAL under different pH condition. The kinetics and FTIR data analysis indicate that the adsorption process is chemisorption. It can be presumed that the adsorption is mainly governed by electrostatic interaction between the coral like Co@Co_3O_4/C adsorbent surface and antibiotics molecules and the π–π interaction coexisting with each other. The significant adsorption efficiency of NAL at pH 6 (scheme 2) is, therefore, primarily caused by the electrostatic attraction between anionic NAL molecules and the positive adsorbent surface. The formation of hydrogen bonding between the adsorbate and adsorbent also plays a pivotal in the adsorption process (Radmehr et al. 2021). Moreover, this concept is further supported by FTIR analysis where a change in intensity in hydroxyl bond after adsorption signifies possible interaction between adsorbent and adsorbate molecules. The adsorption at higher and lower than pH 6 is mainly governed by the π−π interaction between the aromatic groups of NAL and the graphitic carbon present in the carbon network of Co@Co_3O_4/C (Radmehr et al. 2021) which can be further supported by the increase in the intensity of C = C bond at 1620 cm^{-1}.

Reusability of adsorbent

The adsorbents can easily be collected by an external magnet after adsorption and cleaned with an ethanol solution. The mixture is ultrasonicated for 15 min and centrifuges the

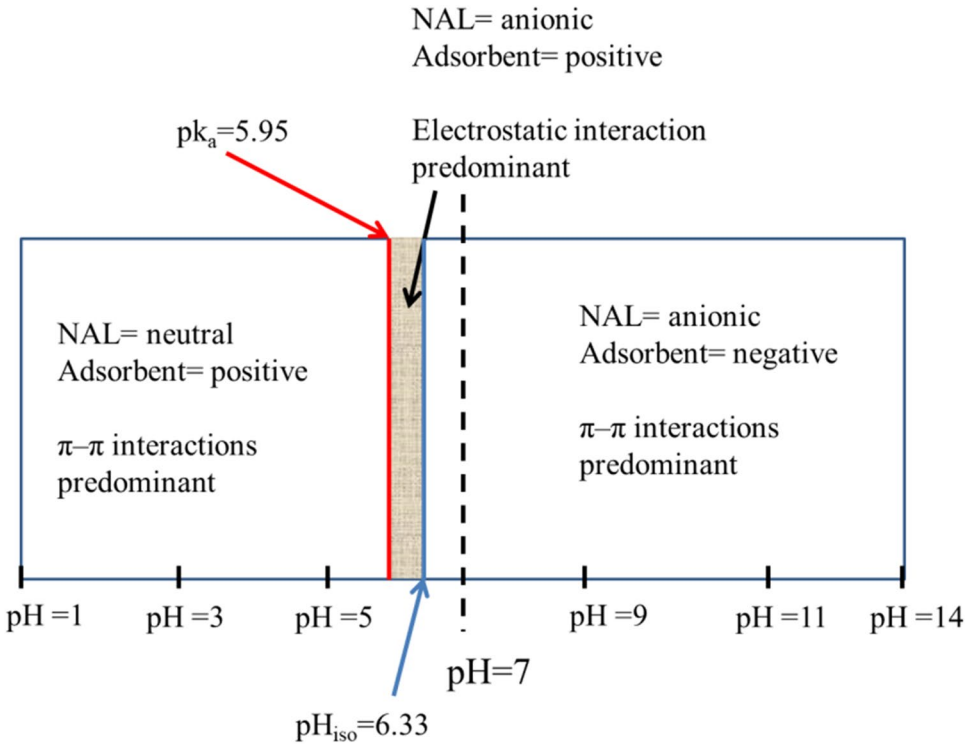

Scheme 2 Schematic representation of surface charge of adsorbent and NAL molecules in different pH

solution. The process is repeated 3–4 times using ethanol to remove the adsorbed NAL completely. Therefore, the regenerated Co@Co_3O_4/C adsorbent is used for evaluating the adsorption efficiencies up to four cycles. After the 4th cycle, the removal efficiency only decreases by 8% illustrated in Fig. 10c. Thus, the adsorbent shows excellent reusability.

Adsorption and selectivity of antibiotics

The coral-like Co@Co_3O_4/C nanohybrid materials are exposed to liquid-phase adsorption in the presence of different class of antibiotics such as NAL, CIP, TC, and SMX. These four antibiotics are chosen from three different classes of antibiotics such as quinolones, tetracyclines, and sulphonamides, respectively. The adsorbent shows very promising results in terms of removal efficiency for each kind of antibiotic. Figure 11 a shows that the Co@Co_3O_4/C adsorbent could remove almost 99.98%, 95.69%, 98.17%, and 66.67% for NAL, CIP, SMX, and TC, respectively. The coral-like Co@Co_3O_4/C nanohybrid adsorbent surface is cationic at pH up to 6.33. The SMX molecule exists as anionic species at pH > 5.7 (Zhang et al. 2011). Therefore, electrostatic interaction between the Co@Co_3O_4/C adsorbent and SMX molecules plays predominant role for the adsorption leading to its 98.17% removal.

However, CIP exists as zwitterion species at 6.1 < pH < 8.7 leading to its high hydrophobicity in this pH rang (Xing et al. 2015). Therefore, the π–π interactions plays the predominant role here where π−π interaction between the aromatic π-electron clouds of CIP molecule and the graphitic carbon present in the carbon network of Co@Co_3O_4/C dominates over the electrostatic force of attraction leading to the higher adsorption of antibiotics over the adsorbent surface (Peng et al. 2016) (Wang et al. 2015).

On the other hand, TC (pk_{a1} = 3.3, pk_{a2} = 7.7, pk_{a3} = 9.7) predominantly exists as cationic species lower pH (Hsu et al. 2018). Therefore, TC molecules experience electrostatic repulsion from the positively charged adsorbent surface resulting in reduced adsorption efficiency. Table S6 shows the comparison of the reported adsorbent with some of the other published literature in terms of their removal of a wide range of antibiotics and ease of separation from the slurry. The coral-like Co@Co_3O_4/C nanohybrid material exhibit versatility in terms of removal of different class of antibiotics and facile magnetic separation simultaneously from the slurry.

A selectivity study on the adsorption performance of Co@Co_3O_4/C adsorbent is depicted for simulated wastewater containing four different antibiotics. The final concentration of each antibiotic such as CIP, NAL, TC, and SMX in simulated wastewater after adsorption is depicted in Fig. 11b. With reference to the initial antibiotic concentration of 15 mg/L, the final concentrations of each antibiotic decrease gradually with time at pH 6. A significant adsorption has been observed for all the antibiotics in just the first minute of the adsorption process. The removal efficiency (Fig. S5) of CIP is approximately ~81%, followed by NAL, TC, and SMX in the first minute of adsorption. The

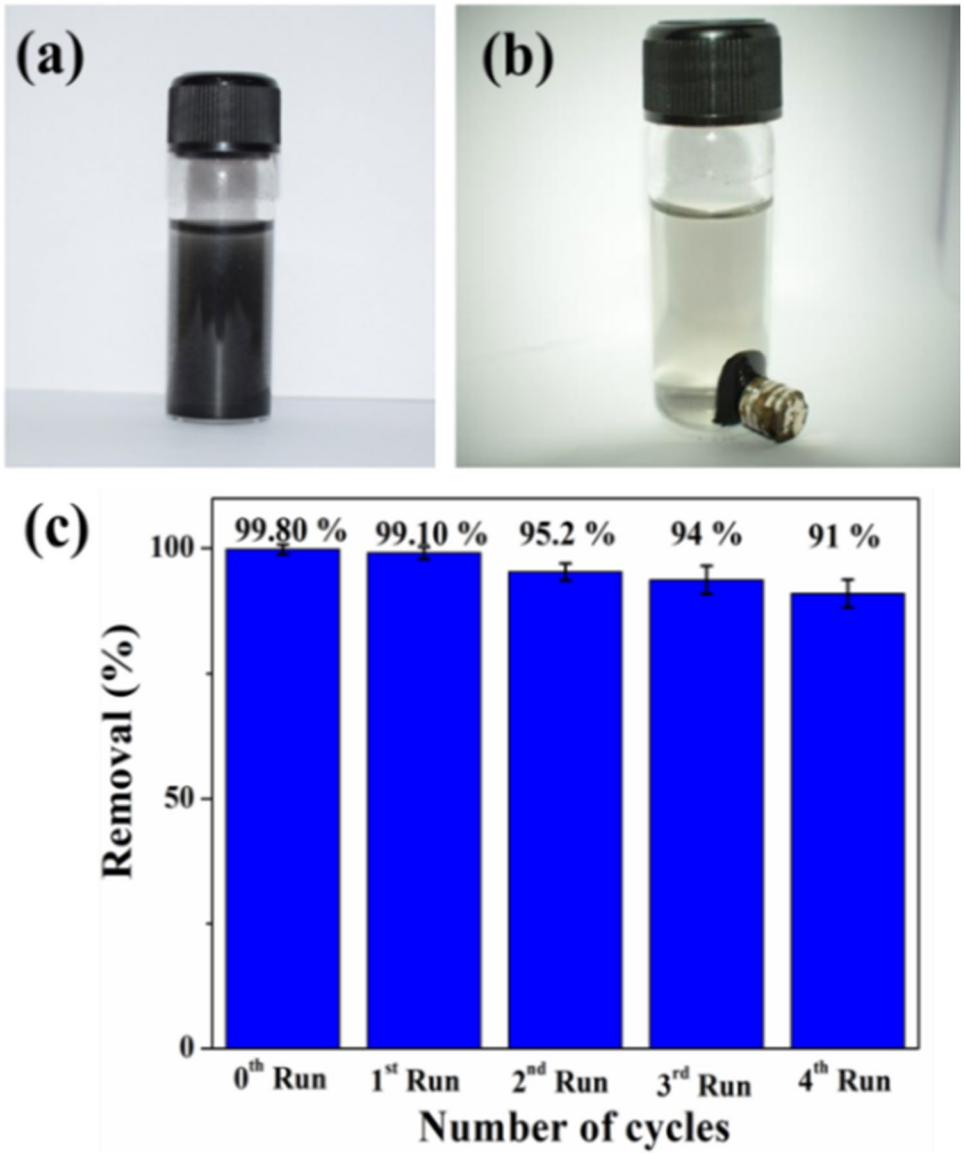

Fig. 10 **a** Optical image of adsorbent in aqueous NAL solution and **b** optical image of magnetic separation of the adsorbent using an external magnet. **c** Reusability of Co@Co_3O_4/C adsorbents for NAL adsorption. Error bars represent the standard deviation of the mean of three experiments

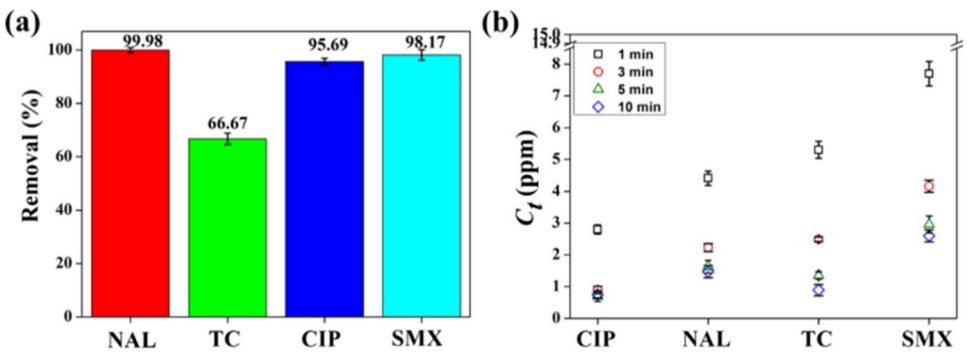

Fig. 11 **a** Comparative studies of adsorption behaviour for different antibiotics at pH 6. Error bars represent the standard deviation of the mean of three experiments. **b** Maximum selectivity of Co@Co_3O_4/C adsorbent for CIP and minimum for SMX in aqueous solution when samples are taken in 1, 3, 5, and 10 min, respectively (The initial concentration is kept at 15 mg/L for each antibiotic)

adsorption process is rather complex for a simulated antibiotic solution with four different kinds of antibiotics coexisting in one system. The properties of antibiotic molecules, as well as the surface qualities of the adsorbent, influence this type of selectivity toward specific antibiotics. The solubility in aqueous solution for zwitterionic CIP is greatly affected by the solution pH and displays very low solubility around pH 6 (Yu et al. 1994). This effect is responsible for

its higher hydrophobicity than three other antibiotics resulting in higher adsorption for CIP through π–π interaction with the adsorbent (Li et al. 2014).

Conclusions

In this research article, we presented a novel coral-like MOF derived Co@Co3O4/C nanohybrids as an outstanding adsorbent material for the treatment of pharmaceutical wastewater. The porous adsorbent facilitates its versatility towards different classes of antibiotics such as quinolones, tetracycline, and sulfonamides with a capability of magnetic separation from the slurry using an external magnetic field. Adsorption studies at various pH levels and surface charge analyses for four different antibiotics reveal interesting pH-sensitive behaviour of the nano-hybrid. A thorough kinetic analysis of the hybrids demonstrates dominant chemisorption, which is further confirmed by XPS and FTIR analysis. More detailed research reveals that the electrostatic and π–π interaction between the Co@Co3O4/C adsorbent and different antibiotic molecules leads to excellent adsorption property of Co@Co3O4/C adsorbent. The adsorbent, however, exhibits selectivity towards CIP in the simulated pharmaceutical wastewater as the CIP molecules' dominant hydrophobic interaction. The outcome of the current research may lead to the development of an innovative pH-sensitive adsorbent for improved pharmaceutical wastewater treatment.

Supplementary Information The online version contains supplementary material available at https://doi.org/10.1007/s11356-023-25846-4.

Acknowledgements The authors highly acknowledge the IIT Delhi CRF facility and IIT Roorkee for its support in characterization of the samples. We thank Ms. Aparna R. K., IISER Trivandrum, for assisting us in characterization facilities. DB acknowledges CIF IIT Guwahati for the experimental support.

Author contributions Puja Bhattacharyya: conceptualization; methodology; investigation; formal analysis; writing original draft, review, and editing; visualization. Prathu Raja Parmar: methodology, formal analysis, resources, review, and editing. Sanchari Basak: methodology, review, and editing, Kashyap Kumar Dubey: analysis, resources, review, and editing. Soumyaditya Sutradhar: analysis, review and editing. Dipankar Bandyopadhyay: funding acquisition, resources, conceptualization, visualization, review and editing, supervision. Sandip Chakrabarti: funding acquisition, conceptualization, visualization, review and editing, supervision.

Funding PB and SC received financial support from the UGC DAE. DB also received financial support from the ICMR grant no. 5/3/8/20/2019-ITR, MeitY grant no. 5(1)/2021-NANO, and CIF IIT Guwahati.

Data availability Not applicable.

Declarations

Ethics approval Not applicable.

Consent to participate Not applicable.

Consent for publication All authors consent to publish this manuscript.

Competing interests The authors declare no competing interests.

References

Ahmed MJ, Hameed BH (2018) Removal of emerging pharmaceutical contaminants by adsorption in a fixed-bed column: a review. Ecotoxicol Environ Saf 149:257–266. https://doi.org/10.1016/j.ecoenv.2017.12.012

Andreozzi R, Canterino M, Marotta R, Paxeus N (2005) Antibiotic removal from wastewaters: the ozonation of amoxicillin. J Hazard Mater 122:243–250. https://doi.org/10.1016/j.jhazmat.2005.03.004

Awad AM, Jalab R, Benamor A et al (2020) Adsorption of organic pollutants by nanomaterial-based adsorbents: an overview. J Mol Liq 301:112335. https://doi.org/10.1016/j.molliq.2019.112335

Bhadra BN, Vinu A, Serre C, Jhung SH (2019) MOF-derived carbonaceous materials enriched with nitrogen: preparation and applications in adsorption and catalysis. Mater Today 25:88–111. https://doi.org/10.1016/j.mattod.2018.10.016

Cao Z, Liu X, Xu J et al (2017) Removal of antibiotic florfenicol by sulfide-modified nanoscale zero-valent iron. Environ Sci Technol 51:11269–11277. https://doi.org/10.1021/acs.est.7b02480

Chen C, Wu A, Yan H et al (2018) Trapping [PMo12O40]3-clusters into pre-synthesized ZIF-67 toward Mo: XCoxC particles confined in uniform carbon polyhedrons for efficient overall water splitting. Chem Sci 9:4746–4755. https://doi.org/10.1039/c8sc01454j

Chen Y, Shi J, Du Q et al (2019) Antibiotic removal by agricultural waste biochars with different forms of iron oxide. RSC Adv 9:14143–14153. https://doi.org/10.1039/c9ra01271k

Choudhary V, Vellingiri K, Thayyil MI, Philip L (2021) Removal of antibiotics from aqueous solutions by electrocatalytic degradation. Environ Sci Nano 8:1133–1176. https://doi.org/10.1039/d0en01276a

Du XD, Wang CC, Liu JG et al (2017) Extensive and selective adsorption of ZIF-67 towards organic dyes: performance and mechanism. J Colloid Interface Sci 506:437–441. https://doi.org/10.1016/j.jcis.2017.07.073

Duraisamy E, Gurunathan P, Das TH et al (2017) [Co(salen)] derived Co/Co3O4 nanoparticle@carbon matrix as high-performance electrode for energy storage applications. J Power Sources 344:103–110. https://doi.org/10.1016/j.jpowsour.2017.01.100

El Bachiri A, Soussi L, Karzazi O et al (2018) Electrochromic and photoluminescence properties of cobalt oxide thin films prepared by spray pyrolysis Electrochromic and photoluminescence properties of cobalt oxide thin films prepared by spray pyrolysis. Spectrosc Lett 52(1):1–8. https://doi.org/10.1080/00387010.2018.1556221

Gao K, Li J, Zhang T et al (2022) The hierarchically nitrogenous magnetic porous carbon prepared by ZIF-67 through mesoporous silica-protected calcination for rapid Cr(VI) removal. Microporous Mesoporous Mater 329:111517. https://doi.org/10.1016/j.micromeso.2021.111517

Garbarino G, Riani P, Lucchini MA et al (2013) Cobalt-based nanoparticles as catalysts for low temperature hydrogen production by ethanol steam reforming. Int J Hydrogen Energy 38:82–91. https://doi.org/10.1016/j.ijhydene.2012.10.054

Guo X, Xing T, Lou Y, Chen J (2016) Controlling ZIF-67 crystals formation through various cobalt sources in aqueous solution. J Solid State Chem 235:107–112. https://doi.org/10.1016/j.jssc.2015.12.021

Hassan N, Shahat A, El-Didamony A, El-Desouky MG, El-Bindary A (2020) Mesoporous iron oxide nano spheres for capturing organic dyes from water sources. Journal of Molecular Structure 1217:128361. https://doi.org/10.1016/j.molstruc.2020.128361

Hedrick SA, Chuang SSC (1998) Temperature programmed decomposition of polypropylene: In situ FTIR coupled with mass spectroscopy study. Thermochim Acta 315:159–168. https://doi.org/10.1016/S0040-6031(98)00283-4

Hsu LC, Liu YT, Syu CH et al (2018) Adsorption of tetracycline on Fe (Hydr)oxides: effects of pH and metal cation (Cu2+, Zn2+ and Al3+) addition in various molar ratios. R Soc Open Sci 5. https://doi.org/10.1098/rsos.171941

Huang X, Tian J, Li Y et al (2020) Preparation of a three-dimensional porous graphene oxide-kaolinite-poly(vinyl alcohol) composite for efficient adsorption and removal of ciprofloxacin. Langmuir 36:10895–10904. https://doi.org/10.1021/acs.langmuir.0c00654

Iervolino G, Zammit I, Vaiano V, Rizzo L (2020) Limitations and prospects for wastewater treatment by UV and visible-light-active heterogeneous photocatalysis: a critical review. Springer International Publishing. https://doi.org/10.1007/978-3-030-49492-6_7

Kiwaan HA, Mohamed FS, El-Ghamaz NA, Beshry NM, El-Bindary A (2021a) Experimental and electrical studies of zeolitic imidazolate framework-8 for the adsorption of different dyes. J Mol Liq 338:116670. https://doi.org/10.1016/j.molliq.2021.116670

Kiwaan HA, Mohamed FS, El-Bindary A, El-Ghamaz NA, Abo-Yassin HR, El-Bindary MA (2021b) Synthesis, identification and application of metal organic framework for removal of industrial cationic dyes. J Mol Liq 342:117435. https://doi.org/10.1016/j.molliq.2021.117435

Li N, Zhou L, Jin X, Owens G, Chen Z (2019) Simultaneous removal of tetracycline and oxytetracycline antibiotics from wastewater using a ZIF-8 metal organic-framework. J Hazard Mater 366:563–572. https://doi.org/10.1016/j.jhazmat.2018.12.047

Li B, Zhang T (2010) Biodegradation and adsorption of antibiotics in the activated sludge process. Environ Sci Technol 44:3468–3473. https://doi.org/10.1021/es903490h

Li H, Zhang D, Han X, Xing B (2014) Adsorption of antibiotic ciprofloxacin on carbon nanotubes: PH dependence and thermodynamics. Chemosphere 95:150–155. https://doi.org/10.1016/j.chemosphere.2013.08.053

Li S, Chen J, Hu S et al (2020) A novel 3D Z-scheme heterojunction photocatalyst: Ag6Si2O7 anchored on flower-like Bi2WO6 and its excellent photocatalytic performance for the degradation of toxic pharmaceutical antibiotics. Inorg Chem Front 7:529–541. https://doi.org/10.1039/c9qi01201j

Li S, Wang C, Liu Y et al (2021) Photocatalytic degradation of antibiotics using a novel Ag/Ag2S/Bi2MoO6 plasmonic p-n heterojunction photocatalyst: mineralization activity, degradation pathways and boosted charge separation mechanism. Chem Eng J 415:128991. https://doi.org/10.1016/j.cej.2021.128991

Li W, Zhang A, Jiang X et al (2017) Low temperature CO_2 methanation: ZIF-67-derived co-based porous carbon catalysts with controlled crystal morphology and size. ACS Sustain Chem Eng 5:7824–7831. https://doi.org/10.1021/acssuschemeng.7b01306

Li X, Zhang W, Liu Y, Li R (2016) Palladium nanoparticles immobilized on magnetic porous carbon derived from ZIF-67 as efficient catalysts for the semihydrogenation of phenylacetylene under extremely mild conditions. ChemCatChem 8:1111–1118. https://doi.org/10.1002/cctc.201501283

Lin KA, Chang H (2015) Chemosphere Ultra-high adsorption capacity of zeolitic imidazole framework-67 (ZIF-67) for removal of malachite green from water. Chemosphere 67:1–8. https://doi.org/10.1016/j.chemosphere.2015.01.041

Meras ID, De La Pena AM, Lopez FS, Caceres MIR (2000) Complexation of antibacterial quinolonic acid and cinolonic derivatives with Zn(II) and Al(III): application to their determination in human urine. Analyst 125:1471–1476. https://doi.org/10.1039/b002512g

Mohebi A, Samadi M, Tavakoli HR, Parastouei K (2020) Homogenous liquid–liquid extraction followed by dispersive liquid–liquid microextraction for the extraction of some antibiotics from milk samples before their determination by HPLC. Microchem J 157:104988. https://doi.org/10.1016/j.microc.2020.104988

Nazari G, Abolghasemi H, Esmaieli M (2016) Batch adsorption of cephalexin antibiotic from aqueous solution by walnut shell-based activated carbon. J Taiwan Inst Chem Eng 58:357–365. https://doi.org/10.1016/j.jtice.2015.06.006

Opriş O, Soran ML, Coman V et al (2013) Determination of some frequently used antibiotics in waste waters using solid phase extraction followed by high performance liquid chromatography with diode array and mass spectrometry detection. Cent Eur J Chem 11:1343–1351. https://doi.org/10.2478/s11532-013-0263-y

Pan Y, Liu Y, Zeng G et al (2011) Rapid synthesis of zeolitic imidazolate framework-8 (ZIF-8) nanocrystals in an aqueous system. Chem Commun 47:2071–2073. https://doi.org/10.1039/c0cc05002d

Park KS, Ni Z, Côté AP et al (2006) Exceptional chemical and thermal stability of zeolitic imidazolate frameworks. Proc Natl Acad Sci U S A 103:10186–10191. https://doi.org/10.1073/pnas.0602439103

Peng B, Chen L, Que C et al (2016) Adsorption of antibiotics on graphene and biochar in aqueous solutions induced by π-π interactions. Sci Rep 6:1–10. https://doi.org/10.1038/srep31920

Pham TD, Le TMA, Pham TMQ et al (2021) Synthesis and characterization of novel hybridized CeO2@SiO_2 nanoparticles based on rice husk and their application in antibiotic removal. Langmuir 37:2963–2973. https://doi.org/10.1021/acs.langmuir.0c03632

Radmehr S, Hosseini Sabzevari M, Ghaedi M et al (2021) Adsorption of nalidixic acid antibiotic using a renewable adsorbent based on graphene oxide from simulated wastewater. J Environ Chem Eng 9:105975. https://doi.org/10.1016/j.jece.2021.105975

Rashidi Nodeh H, Sereshti H (2016) Synthesis of magnetic graphene oxide doped with strontium titanium trioxide nanoparticles as a nanocomposite for the removal of antibiotics from aqueous media. RSC Adv 6:89953–89965. https://doi.org/10.1039/c6ra18341g

Senthil Kumar P, Vincent C, Kirthika K, Sathish Kumar K (2010) Kinetics and equilibrium studies of Pb2+ ion removal from aqueous solutions by use of nano-silversol-coated activated carbon. Brazilian J Chem Eng 27:339–346. https://doi.org/10.1590/s0104-66322010000200012

Sharma M, Joshi M (2019) ZnO tetrapods and activated carbon based hybrid composite: adsorbents for enhanced decontamination of hexavalent chromium from aqueous solution. Chem Eng J 358:540–551. https://doi.org/10.1016/j.cej.2018.10.031

Shahabuddin S, Sarih NM, Mohamad S, Atika Baharin SN (2016) Synthesis and characterization of Co_3O_4 nanocube-doped polyaniline nanocomposites with enhanced methyl orange adsorption from aqueous solution. RSC Adv 6:43388–43400. https://doi.org/10.1039/c6ra04757b

Suhag D, Singh A, Chattopadhyay S et al (2015) Hydrothermal synthesis of nitrogen doped graphene nanosheets from carbon nanosheets with enhanced electrocatalytic properties. RSC Adv 5:39705–39713. https://doi.org/10.1039/c5ra05060j

Thi N, Tu T, Thien TV et al (2018) Adsorptive removal of Congo red from aqueous solution using zeolitic imidazolate framework–67. Biochem Pharmacol 6(2):2269–2280. https://doi.org/10.1016/j.jece.2018.03.031

Wang C, Kim J, Tang J et al (2020a) New strategies for novel MOF-derived carbon materials based on nanoarchitectures. Chem 6:19–40. https://doi.org/10.1016/j.chempr.2019.09.005

Wang G, Zhang Y, Wang S et al (2020b) Adsorption performance and mechanism of antibiotics from aqueous solutions on porous

boron nitride-carbon nanosheets. Environ Sci Water Res Technol 6:1568–1575. https://doi.org/10.1039/d0ew00117a
Wang W, Chakrabarti S, Chen Z et al (2014) A novel bottom-up solvothermal synthesis of carbon nanosheets. J Mater Chem A 2:2390–2396. https://doi.org/10.1039/c3ta13593d
Wang X, Qin Y, Zhu L, Tang H (2015) Nitrogen-doped reduced graphene oxide as a bifunctional material for removing bisphenols: Synergistic effect between adsorption and catalysis. Environ Sci Technol 49:6855–6864. https://doi.org/10.1021/acs.est.5b01059
Wang Y, Hao J, Li W et al (2020c) Mn_3O_4/$Co(OH)_2$ cactus-type nanoarrays for high-energy-density asymmetric supercapacitors. J Mater Sci 55:724–737. https://doi.org/10.1007/s10853-019-03998-4
Wu Q, Li Z, Hong H (2013) Adsorption of the quinolone antibiotic nalidixic acid onto montmorillonite and kaolinite. Appl Clay Sci 74:66–73. https://doi.org/10.1016/j.clay.2012.09.026
Wu Y, Chen Z, Cheong WC et al (2019) Nitrogen-coordinated cobalt nanocrystals for oxidative dehydrogenation and hydrogenation of N-heterocycles. Chem Sci 10:5345–5352. https://doi.org/10.1039/c9sc00475k
Xing X, Feng J, Lv G et al (2015) Adsorption mechanism of ciprofloxacin from water by synthesized birnessite. Adv Mater Sci Eng 2015. https://doi.org/10.1155/2015/148423
Yang W, Li X, Li Y et al (2019) Applications of metal–organic-framework-derived carbon materials. Adv Mater 31:1–35. https://doi.org/10.1002/adma.201804740
Yu X, Zipp GL, Ray Davidson IIIGW (1994) The effect of temperature and pH on the solubility of quinolone compounds. Pharm. Res. 11:522–527
Zhang D, Pan B, Wu M et al (2011) Adsorption of sulfamethoxazole on functionalized carbon nanotubes as affected by cations and anions. Environ Pollut 159:2616–2621. https://doi.org/10.1016/j.envpol.2011.05.036
Zhao Y, Tang JJ, Motavalizadehkakhky A et al (2019) Synthesis and characterization of a novel CNT-FeNi3/DFNS/Cu(ii) magnetic nanocomposite for the photocatalytic degradation of tetracycline in wastewater. RSC Adv 9:35022–35032. https://doi.org/10.1039/c9ra05817f
Zhou F, Yu T, Du R et al (2020) Clinical course and risk factors for mortality of adult inpatients with COVID-19 in Wuhan, China: a retrospective cohort study. Lancet 395:1054–1062. https://doi.org/10.1016/S0140-6736(20)30566-3